Comparison of Two Sensor Data Fusion Methods in a Tightly Coupled UWB/IMU 3-D Localization System

3 authors:

Giovanni Miraglia
The MathWorks, Inc
8 PUBLICATIONS   **25** CITATIONS

SEE PROFILE

Khashyar Niki Maleki
University of Tulsa
13 PUBLICATIONS   **155** CITATIONS

SEE PROFILE

Loyd Reed Hook
University of Tulsa
37 PUBLICATIONS   **187** CITATIONS

SEE PROFILE

Some of the authors of this publication are also working on these related projects:

Decision Making, Coordination, and Control of Soccer Playing Robots in Non-deterministic environment View project

Initial designs for an automatic forced landing system for safer inclusion of small unmanned air vehicles into the national airspace View project

Comparison of Two Sensor Data Fusion Methods in a Tightly Coupled UWB/IMU 3-D Localization System

Giovanni Miraglia, K. Niki Maleki, Loyd R. Hook

Electrical and Computer Engineering

The University of Tulsa

Tulsa, Oklahoma, USA

giovmi@utulsa.edu; niki-maleki@utulsa.edu; loyd-hook@utulsa.edu

Abstract— **There currently exists a high demand for vehicles with ever increasing levels of autonomy. While some of these vehicles may depend on GPS for localization, other vehicles will require a more precise localization solution in order to perform their tasks. In addition, some vehicles may need to work in GPS denied environments. These issues could be addressed with the use of an Ultra-Wide Band (UWB) ranging sensor fused with an Inertial-Measurement-Unit (IMU) using an Extended Kalman Filter (EKF). The main goal of this work is to investigate and compare two different sensor data fusion techniques to incorporate a 3-axis 9-DOF IMU in a tightly coupled fashion to a 3-D positioning solution that is derived from UWB signals. The techniques differ from each other in that the first fusion of the IMU data occurs in the prediction step and the second fusion occurs in the update step. Experimental results obtained with a quadcopter show that the data fusion performed in the update step outperforms the fusion performed in the prediction step. The results also show that when using very accurate UWB ranging sensors, the use of IMU data does not improve significantly the accuracy of the position. However, the integration of IMU data in the update step increases the robustness of the EKF against erroneous modelling of the process noise.**

Keywords— Kalman filter; sensor fusion; localization; IMU; UWB.

I. Introduction

It is becoming increasingly clear that to realize the full potential of unmanned vehicles, higher levels of autonomy than is currently available will be required. This is due to several factors, but is a direct result of the incredible diversity and usefulness of their possible functions. However, removing the human pilot from the control loop also removes the human's sensing and localization abilities as well. These functions will need to be replaced by electrical and mechanical sensors whose output data is processed to provide a localization solution with the level of precision required of the control task. For typical airplane applications, GPS may be able to provide this level of localization precision. However, for small or medium sized UAVs, which operate in areas which are much smaller than a traditional airplane could operate, GPS may not be able to provide a precise enough solution. One particularly interesting example scenario involves the use of UAVs indoors where the size of the work area is very small, compared to normal airplane operations, and GPS signals are not available. Another very relevant example is that of a small UAV flying in close proximity to buildings, people, or other UAVs. In addition, other autonomous vehicles will almost certainly require a more precise localization solution as well. For example, the relative distances between cars on a roadway or between the road and obstacles or dangerous areas is too small to allow a GPS only positioning solution. These examples, and others, provide the motivation for the work presented in this paper. In order to fully appreciate the problem, the indoor environment and a UAV was chosen for experimentation; however, the results offered here are applicable to other outdoor scenarios as well.

Several technologies have been suggested to build indoor positioning systems. In [1] and [2] comprehensive surveys of different technologies and algorithms are compared. In both works, relative distance measurements using Ultra-Wide Band (UWB) raging radar units appear to be the most appealing technology. UWB signals are particularly suitable for indoor localization systems due to their high accuracy and ability to operate in other than strictly Line-of-Sight (LOS) conditions. For instance, in [3] a 2-D UWB positioning system that has an accuracy of less than 4 cm is described. When compared to a nominal GPS accuracy of 3 m the UWB provides superior results. Better accuracies could be achieved with optical positioning systems that are based on the use of Infrared (IR) cameras. In that case, the drawback is that LOS to the tracking reflectors is required. Unlike infrared signals, UWB signals can easily penetrate different kinds of material thanks to the large bandwidth [2]. Furthermore, the large bandwidth also allows precise distance measurement even in presence of multipath [4]. Other advantages are the low power used in the UWB transmissions and the robustness against radio interference [1].

One of the available UWB commercial systems is the PulsoOn 440 manufactured by Time Domain. This device can estimate distances by using the so called "Two-Ways-Time-of-Fly" (TWToF), which allows distance estimation between two nodes without requiring synchronization between them [5]. A node A estimates the distance from node B as follows:

a) Node A sends a request to node B;

b) Node B receives the request from node A;

c) Node B sends the answer to node A;

d) Node A receives the answer.

Denoting the elapsed time between the steps a and d with τ_{tot} and the one elapsed between the steps b and c with τ_{delay}, the distance between the two nodes is:

$$d=\frac{c}{2}(\tau_{tot}-\tau_{delay}), \quad c=\text{speed of light} \qquad (1)$$

As explained in [1] and [2], in general different technologies require different algorithms, and even two different uses of the same technology might require different algorithms as well. In the case of UWB positioning systems, a certain number of fixed nodes (anchors) are deployed in known locations. To obtain the 3-D position, at least four anchors must be used. If the anchors and the mobile node are synchronized, the mobile node can be localized in the space by using simple trilateration techniques and the least square method [2]. If the anchors and the mobile node are standalone devices, the trilateration cannot be applied because the distances are not measured at the same time. This is the case of the Time Domain modules[1], which consequentially require the use of a different algorithm. In this work, the localization is performed by using the Kalman Filter in its linearized form, which is referred to as Extended Kalman Filter (EKF). One of the key points of the EKF is the underlying state transition model, which in this case is a motion model. The solution presented in [5] uses a constant velocity (CV) motion model; however, the drawback of using a CV model is that in presence of a target having strong accelerations, the EKF could work as a low pass filter. For that reason, in this work a constant acceleration (CA) motion model has been utilized. Nevertheless, with a CA motion model, sometimes the EKF could interpret the noise as acceleration. To counteract this phenomenon, the EKF could be improved by integrating an Inertial Measurement Unit (IMU) that provides the actual accelerations.

The main goal of this research is to evaluate the benefits that the addition of IMU data can provide in terms of position accuracy in a UWB localization system. The target application of this localization system is the localization of an Unmanned Aerial Vehicle (UAV), such as a drone or a Radio Controlled (RC) airplane. In this work, a tightly coupled architecture is considered to integrate the IMU data with the UWB data for the position estimation. There are two approaches to fuse the accelerations provided by the IMU. The first one is to fuse the data in the prediction step of the EKF, which means to utilize the values provided by the gyroscope and the accelerometer as essentially a control input. An example of such techniques can be found in [6], where an EKF is used to estimate the attitude of an RC airplane. In this case, the gyroscope and accelerometer data are used as control input in the prediction step, while the velocity provided by a GPS receiver is used in the update step to correct the prediction. Moreover, in the system described in [7], IMU data are fused with UWB data in the prediction step. However, in this system only the 2-D position is computed and, different from our system, the UWB module provides coordinates rather than simple distances. In our implementation of this first fusion technique, the gyroscope and the accelerometer data are both utilized as control inputs in the prediction step, while the correction is performed by using the distances provided by the UWB module. Furthermore, different from the work presented in [6], we are only interested in the estimation of the position.

The second possible approach is known as measurement fusion method [8], which in its simplest form consists in merging the multi-sensor data through the observation vector. In our case, this type of sensor fusion implies that the prediction is totally based on a mathematical motion model, while the correction is performed employing both the IMU data and the UWB data.

The paper is organized as follows. The second section provides a theoretical background about the Extended Kalman Filter. The details of the specific implementation of the EKF for the localization problem and for the two sensor data fusion methods are given in section three. Furthermore, in section three there is also a brief description of the filtering techniques used to improve the quality of the localization and it is explained how the anchors were deployed in the environment. The equipment that was employed for experimentation is described in section four and the experimental results are presented in the fifth section.

II. Extended Kalman Filter

The linear Kalman filter is based on the use of a state evolution model and an observation model

$$x_{k+1}=F_k x_k+B_k u_k+w_k \qquad (2)$$

$$z_k=H_k x_k+v_k \qquad (3)$$

where x_k is the state vector, u_k is the input vector, z_k is the observation vector, F_k is the transition matrix, B_k is the control input matrix and H_k is the observation matrix. The terms w_k and v_k respectively denote the process noise vector and the sensor noise vector, and they are both zero-mean white Gaussian random vectors [9]. The Kalman Filter performs the state estimation in two steps, which are prediction and update. In the prediction step the new state and its covariance matrix P_k are predicted by using the previous state, the previous covariance matrix and the current input. In the update step the predicted state and the predicted covariance matrix are corrected by using the current observation vector.

Prediction:

$$\hat{x}_{k|k-1}=F_k \hat{x}_{k-1|k-1}+B_k u_k \qquad (4)$$

$$P_{k|k-1} = F_k P_{k-1|k-1} F_k^T + Q_k \qquad (5)$$

Update:

$$\tilde{y}_k=z_k-H_k \hat{x}_{k|k-1} \qquad (6)$$

$$S_k=H_k P_{k|k-1} H_k^T+R_k \qquad (7)$$

$$K_k=P_{k|k-1} H_k^T S_k^{-1} \qquad (8)$$

$$\hat{x}_{k|k}=\hat{x}_{k|k-1}+K_k \tilde{y}_k \qquad (9)$$

$$P_{k|k}=(I-K_k H_k)P_{k|k-1} \qquad (10)$$

In the equations (6-10), k|k-1 means that the value is predicted by using the knowledge of the previous value, while k|k is used for the corrected values. The matrix Q_k is the covariance matrix of the process noise w_k, R_k is the covariance matrix of the sensor noise v_k, $\tilde{y}_k$ is the innovation and K_k is the Kalman Gain. These equations can be extended to nonlinear

---

[1] These modules can be synchronized to work in a TDMA network, in which a slot map defines which modules must communicate. But even in that case one node can measure only one distance at a time.

systems in which either the evolution model or the observation model is nonlinear.

$$x_k = f(x_{k-1}, u_{k-1}, w_{k-1}) \tag{11}$$

$$z_k = h(x_k, v_k) \tag{12}$$

To apply the Kalman Filter in this case, it is required that $f(x_{k-1}, u_{k-1}, w_{k-1})$ and $h(x_k, v_k)$ are continuously differentiable in x_k [9]. If the condition is satisfied, (4) and (6) are replaced by (13) and (14).

$$\hat{x}_{k|k-1} = f(\hat{x}_{k-1|k-1}, u_{k-1}) \tag{13}$$

$$\tilde{y}_k = z_k - h(\hat{x}_{k|k-1}) \tag{14}$$

In this case, F_k and H_k are the Jacobian matrix of the functions $f(\hat{x}_{k-1|k-1}, u_{k-1})$ and $h(x_k, v_k)$. In the first case, the Jacobian is computed by using the previous state, while in the second case the prediction of the new state is used.

$$F_k = \left. \frac{\partial f}{\partial x} \right|_{\hat{x}_{k-1|k-1}} \tag{15}$$

$$H_k = \left. \frac{\partial h}{\partial x} \right|_{\hat{x}_{k|k-1}} \tag{16}$$

III. Localization Algorithms

In this section, the theoretical formulation of the EKF for the UWB localization system is discussed. Furthermore, the implementation of the two sensor data fusion techniques that have been evaluated in this work is illustrated. Finally, it is explained how the raw data delivered by the IMU and the UWB ranging sensor are filtered and how the anchors are placed to improve the quality of the system.

A. UWB data only

Since the EKF is applied to localize a target, in this case the state transition model is a motion model. In [10] different motion models are presented and the one used here is the variant of the CA motion model referred to as "white-noise jerk model". In this model, the acceleration is assumed to be affected by a white noise with power spectral density S_w. Furthermore, in this model the movements along the three axes are assumed to be decoupled. The discrete representation of this motion model for a single coordinate is:

$$x_k = Fx_{k-1} + w_k, \quad F = \begin{bmatrix} 1 & t & \frac{t^2}{2} \\ 0 & 1 & t \\ 0 & 0 & 1 \end{bmatrix} \tag{17}$$

$$x_k = \begin{bmatrix} x \\ \dot{x} \\ \ddot{x} \end{bmatrix}, \quad Q = cov(w_k) = S_w \begin{bmatrix} \frac{t^5}{20} & \frac{t^4}{8} & \frac{t^3}{6} \\ \frac{t^4}{8} & \frac{t^3}{3} & \frac{t^2}{2} \\ \frac{t^3}{6} & \frac{t^2}{2} & t \end{bmatrix} \tag{18}$$

In the above representation $x, \dot{x}, \ddot{x}$ are respectively the general coordinate, speed, and acceleration and t is the time elapsed between the previous state and the current state. The above

model can be extended to the 3-D case by employing the fact that the motions along the three axes are decoupled:

$$x_{3D_k} = F_{3D} x_{3D_{k-1}} + w_{3D_k} \tag{19}$$

$$x_{3D_k} = [x \; v_x \; a_x \; y \; v_y \; a_y \; z \; v_z \; a_z]^T, \; F_{3D} = diag[F \; F \; F] \tag{20}$$

$$Q_{3D} = cov(w_{3D_k}) = diag[Q \; Q \; Q] \tag{21}$$

When only UWB modules are used, the only available information for the update step is the distance between the target and a reference location. In this case z_k, R_k, S_k, K_k are scalars, the observation function is $h(x_{k|k-1}): R^3 \rightarrow R$, and H_k is a vector of nine elements.

$$h(x,y,z) = \sqrt{(x-x_a)^2 + (y-y_a)^2 + (z-x_a)^2} \tag{22}$$

$$H = \left[\frac{(x-x_a)}{h(x,y,z)} \; 0 \; 0 \; \frac{(y-y_a)}{h(x,y,z)} \; 0 \; 0 \; \frac{(x-x_a)}{h(x,y,z)} \; 0 \; 0 \right] \tag{23}$$

The values x_a, y_a, z_a are the coordinates of the anchor from which the distance is measured.

B. UWB data and IMU data fused in the prediction step

When fusing IMU data in the prediction step, both the transition model and the observation model are nonlinear; thus, (15) and (16) must be used. In this kind of fusion, the data coming from the accelerometer and the gyroscope are used as input in the state transition model. Unlike the previous case, here the CA motion model is no longer employed; thus, the are no accelerations in the state. On the other hand, the state must include information about the attitude of the target to allow the transformation of the accelerations provided by the IMU from the body frame to the inertial frame. That can be done essentially in two ways: quaternions or Euler angles. Here, Euler angles are used, and in (24) ϕ, θ, and ψ are respectively roll, pitch, and yaw angles.

$$x_{FP_k} = [x \; v_x \; y \; v_y \; z \; v_z \phi \; \theta \; \psi]^T \tag{24}$$

The state transition function is the following:

$$\hat{x}_{k|k-1} = f(\hat{x}_{k-1|k-1}, u_{k-1}) = A\hat{x}_{k-1|k-1} + T(M_B^I u_{k-1} - \vec{g}) \tag{25}$$

Where:

$$A = diag[F' \; F' \; F' \; I_{3x3}], \; F' = \begin{bmatrix} 1 & t \\ 0 & 1 \end{bmatrix} \tag{26}$$

$$T = diag[T' \; T' \; T' \; I_{3x3}], \; T' = \begin{bmatrix} \frac{t^2}{2} & 0 \\ 0 & t \end{bmatrix} \tag{27}$$

$$u_{k-1} = [acc_x \; acc_y \; acc_z \; gyro_x \; gyro_y \; gyro_z]^T \tag{28}$$

$$\vec{g} = [0 \; 0 \; 0 \; 0 \; g \; g \; 0 \; 0 \; 0]^T \tag{29}$$

The nonlinearity in the transition function is due to the presence of the matrix M_B^I, which is the transformation matrix that is used to transform the input vector from the body frame to

the inertial frame. The elements of M_B^I are functions of the angles ϕ, θ, and ψ. The product $M_B^I u_{k-1}$ is a vector having nine elements as the state vector x_k.

In this case, the covariance matrix of the process noise has the same structure as of the CV motion model. In (30) and (31), Q_{FP_t} is the portion of the covariance matrix associated with a single translational movement; while, Q_{FP_r} is the portion associated with the three rotations. The subscript FP stands for "Fusion in the Prediction step".

$$Q_{FP}=\text{cov}\left(w_{FP_k}\right)=\text{diag}\left[Q_{FP_t}\ Q_{FP_t}\ Q_{FP_t}\ Q_{FP_r}\right] \quad (30)$$

$$Q_{FP_t}=S_{w_t}\begin{bmatrix}\dfrac{t^4}{4} & \dfrac{t^3}{2}\\[2mm]\dfrac{t^3}{2} & t^2\end{bmatrix},\ Q_{FP_r}=S_{w_r}\begin{bmatrix}t^2 & 0 & 0\\0 & t^2 & 0\\0 & 0 & t^2\end{bmatrix} \quad (31)$$

Since the fusion is performed in the prediction step, the observation model is the same as the case in which only UWB data are used, thus (22) and (23) are used.

C. UWB data and IMU data fused in the update step

For the fusion performed through the observation vector, the prediction step is the same as the case in which only UWB data are used; therefore, the transition model is linear. However, in this case the state has fifteen elements because it must include both the Euler angles and the turn rates. As a result, in the prediction step the EKF estimates both accelerations and turn rates.

$$x_{FU_k}=\left[x\ v_x\ a_x\ y\ v_y a_y\ z\ v_z\ a_z\ \phi\ p\ \theta\ q\ \psi\ r\right]^T \quad (32)$$

$$x_{FU_k}=F_{FU}x_{FU_{k-1}}+w_{FU_k} \quad (33)$$

$$F_{FU}=\text{diag}\left[F\ \ F\ \ F\ \ F'\ \ F'\ \ F'\right] \quad (34)$$

$$Q_{FU}=\text{cov}\left(w_{FU_k}\right)=\text{diag}\left[Q\ Q\ Q\ Q_{FP_t}Q_{FP_t}Q_{FP_t}\right] \quad (35)$$

In the equations (32-35), FU stands for "Fusion in the Update step". The transition matrix and the covariance matrix in this case are built by utilizing the CA model for the translational motion and the CV model for the rotational motion.

In this case, in the update step there is no longer a single measure; instead, there is a vector of measures, which contains the distance obtained with the UWB module and the acceleration and turn rates obtained with the IMU. Therefore, the observation function is $h_{FU}(x_{k|k-1}):R^{15}\to R^7$.

$$z_{FU_k}=\left[d_{UWB}\ acc_x\ acc_y\ acc_z\ gyro_x\ gyro_y\ gyro_z\right]^T \quad (36)$$

$$h_{FU}\left(\hat{x}_{FU_{k|k-1}}\right)=\left[h(x,y,z)\ a_{x_T}\ a_{y_T}\ a_{z_T}\ p_T\ q_T\ r_T\right]^T \quad (37)$$

$$\left[a_{x_T}\ a_{y_T}\ a_{z_T}\ p_T\ q_T\ r_T\right]^T=M_I^B\left[a_x\ a_y\ a_z\ p\ q\ r\right]^T \quad (38)$$

In (37) and (38) the subscript T stands for transformed and the values with that subscript are the accelerations and turn rates

transformed from the inertial frame to the body frame employing the matrix M_I^B. Furthermore, since seven values are used in the correction step, the measurement noise is defined by the covariance matrix R_{FU_k}.

$$R_{FU_k}=\text{diag}\left[\sigma_{UWB}^2\ \sigma_{ACC}^2\ \sigma_{ACC}^2\ \sigma_{ACC}^2\ \sigma_{GYRO}^2\ \sigma_{GYRO}^2\ \sigma_{GYRO}^2\right] \quad (39)$$

It is worth to notice that in this second fusion technique, the computational cost is much higher. In fact, the state has a higher dimension, and since there is a vector of measures rather than a single value, R_{FU_k} is a 7x7 matrix, and H_{FU} is a 7x15 matrix computed by utilizing the (16).

D. Data prefiltering and placement of the anchors

Low cost IMUs, which are typically found on small UAVs, are known to be especially noisy. To improve the quality of the signals coming from the accelerometer and the gyroscope, a six-point moving average filter is used. While for IMU it was possible to apply a filtering technique to improve the quality of the signals, that was not possible for the distances measured with the UWB modules. That was due to the low update rate of the distances. However, those modules have a pretty narrow dynamic range, which in our tests was found to be approximatively 5 cm in favorable conditions and 10 cm in a high multipath environment. On the other hand, certain unpredictable circumstances, such as severe Non-Line-of-Sight (NLOS) condition, might cause a distance to be completely erroneous. Unfortunately, a single outlier can cause the EKF to oscillate for several time steps. To overcome this issue, an outlier detector based on the average estimated velocity is used.

When setting the system, a very important aspect that must be considered is the dilution of precision. This phenomenon is illustrated in [11], where the author explains how the position of the anchors affects the accuracy of the localization system. In particular, it is shown that the placement of the anchors in a plane that is parallel to the ground (i.e. anchors placed at the same altitude) leads to a low accuracy in the altitude estimation. For that reason, our first setup consisted of six anchors, placed in two different planes parallel to the ground. However, since the first configuration was unsatisfying, a second configuration with five anchors deployed in three different planes was used.

IV. EQUIPMENT AND SETUP

The data collection was performed in a pool area by using the quadcopter DJI Phantom 3. To have a reference system to compare the different approaches, a very accurate (<1 mm [12]) optical tracking system was used. Such a system is called Optitrack and is manufactured by Natural Point. Optitrack consists of several Infra-Red (IR) detecting cameras (in this research 8 Flex-13 cameras were employed) and IR reflecting objects. The tracked object is equipped with a unique pre-determined pattern of IR reflecting/emitting points referred to as "Rigid Body". In our tests, to have a better tracking quality, the quadcopter was equipped with four IR LEDs, thus active IR sources were used.

The IMU data were collected by using two diverse sources. One was the VMU931 manufactured by Variense. This device is equipped with a gyroscope, an accelerometer and a

magnetometer. The second source was a Pixhawk autopilot, which is a system manufactured by 3DRobotics. This platform has advanced 32-bit ARM Cortex M4 processor for high volume real time computation, 168 MHz 256 KB RAM with 2MB flash memory as the main memory, and more importantly, it uses high precision IMU that consists of the following sensors: ST Micro L3GD20 3-axis 16-bit gyroscope, ST Micro LSM303D 3-axis 14-bit accelerometer and magnetometer, redundant with Invensense MPU 6000 3-axis accelerometer and gyroscope. The choice of using two diverse sources for the IMU data was due to the need of having redundant information. In fact, the data of the VMU931 were noisier than the Pixhawk data, on the other hand the Pixhawk data were affected by a bias error.

The UWB ranging sensor used in this work was the PulsON 440, which is manufactured by Time Domain. This is a UWB module that can work as a precise ranging radio or radar sensor in high multipath and highly reflective environments. Its maximum operating range varies from 300 m to 1100 m, depending on antenna height and ground surface characteristics.

Finally, the last component was the Raspberry Pi 3 rev. B, which is a single board computer equipped with a 1.2 GHz 64-bit quad-core ARMv8 CPU, 1 GB RAM and that can support several operating systems. In our case the used operating system was Raspbian, which is based on Debian. Even though, we do have a real-time version of our localization system that runs on the Raspberry Pi, in the final test the Raspberry Pi was used just to collect the raw data from the UWB module and the IMUs. The data were then post-processed by using the software MATLAB.

V. EXPERIMENTAL RESULTS

This section demonstrates the results that were obtained in our experiments. Initially, the three different approaches were tested by using the configuration 1 that is shown in Fig. 2. In this first configuration, the anchors were placed at two different altitudes, and there were three different x values and two different y values. However, the results revealed that for the z coordinate there was clearly a problem. In fact, in Fig. 3 it is possible to notice that the z coordinate was affected by a drift error. Furthermore, Fig. 4, which is a zoomed view of Fig. 3, is a typical example in which the use of IMU data is useful. In fact, it is possible to notice that the use of IMU reduces the oscillations caused by strong accelerations considerably. On the other hand, Fig. 5 and Fig. 6 show that the accuracy in the horizontal plane was satisfactory. That was because in the

horizontal plane, the anchors were placed in a more scattered manner than the vertical plane.

To improve the quality of the localization, the configuration of the anchors was changed. The second configuration had five anchors distributed on three different altitudes, and with three x values and three y values. In Fig. 7, Fig. 8, and Fig. 9 there are the coordinate obtained with the configuration 2. In this case, the improvement of the quality of the localization is completely noticeable.

The evaluation of the three approaches was performed by comparing the obtained tracks with the one obtained with the optical system. Since the Optitrack had an update frequency of 100 Hz, while our UWB localization systems had un update
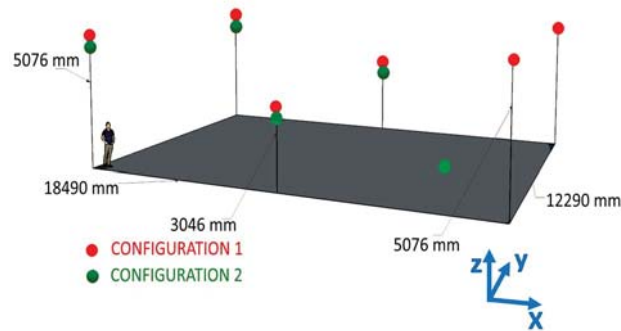

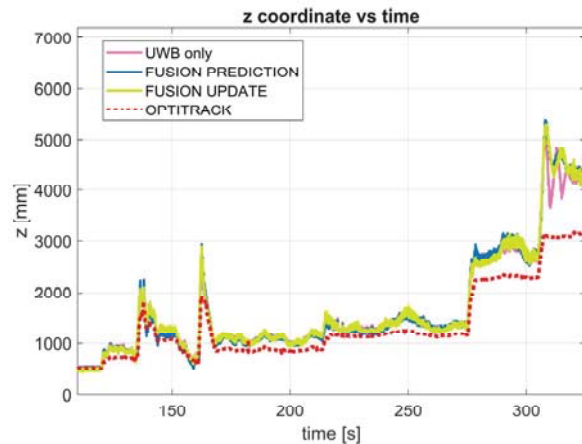
Fig. 2: position of the anchors.
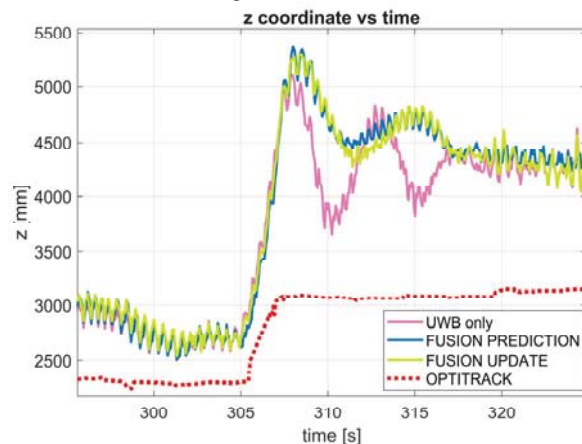

Fig. 3: z coordinate with configuration 1.

Fig. 4: oscillation of z coordinate with configuration 1

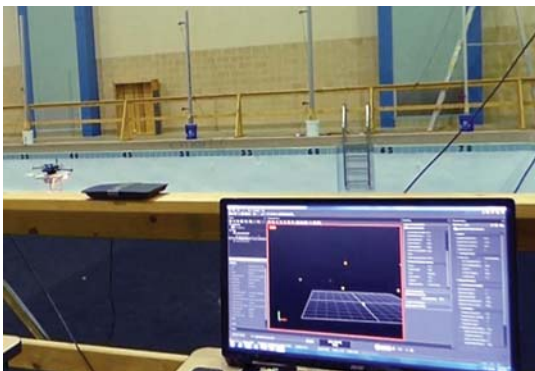Fig. 1: data collection session.

Fig. 5: x coordinate with configuration 1.

Fig. 7: z coordinate with configuration 2.

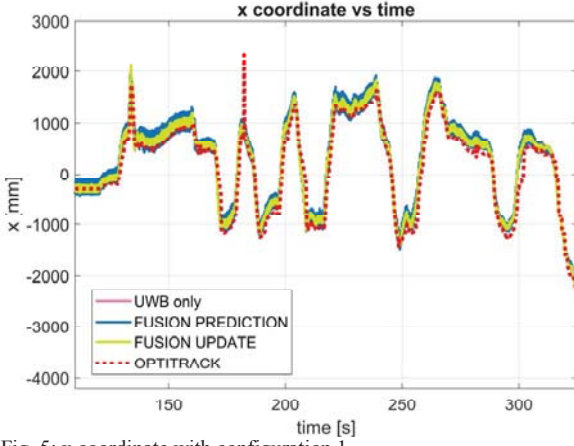Fig. 6: y coordinate with configuration 1.
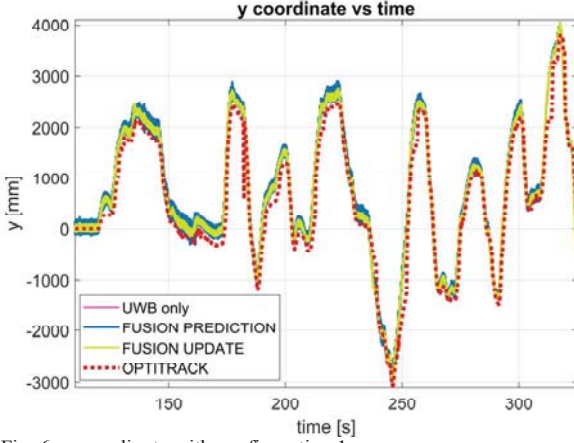

Fig. 8: x coordinate with configuration 2.

Fig. 9: y coordinate with configuration 2.

frequency that oscillated between 10 Hz and 16 Hz, the comparison with the Optitrack was performed by sampling the Optitrack data with a variable sample frequency. Furthermore, to obtain the Probability Distribution Function (PDF) of the error, only time intervals in which the Optitrack data were very accurate were used. To have the most comprehensive investigation possible, the data collection was performed by piloting the drone with different speeds, accelerations, and trajectories. The PDFs of the error for the three approaches are shown in Fig. 10, Fig. 11, and Fig. 12. The results show that the position provided by the system that fuses the IMU data in the update step is just slightly better than the one provided by the systems that uses only UWB data. In fact, while in the former the peak of the distribution is between 12 cm and 18 cm, for the latter the peak is between 15 cm and 21cm. On the other hand, the fusion of IMU data performed in the prediction step provides a less accurate position. In this case, the PDF of the error is spread over a broader range of error values and the peak is between 18 cm and 27 cm.

One of the most crucial factors in the implementation of a Kalman Filter is the tuning process, which consists in finding the optimal values for the covariance matrix of the process noise and the covariance matrix of the observation noise. For the second one, that means to find the values for the matrix R_{FU_k}, which usually is a diagonal matrix whose values are the variances of the sensors. Therefore, if the variances of the sensors are known,
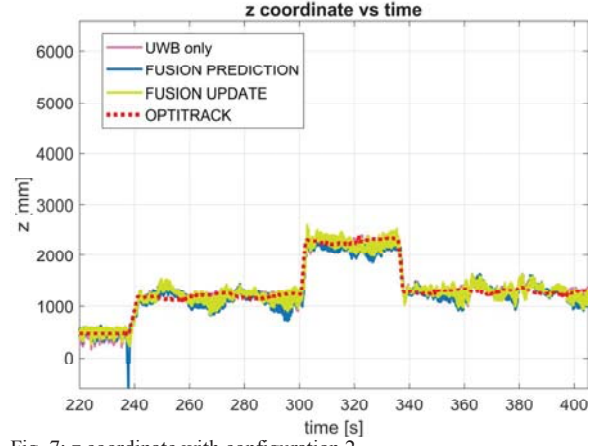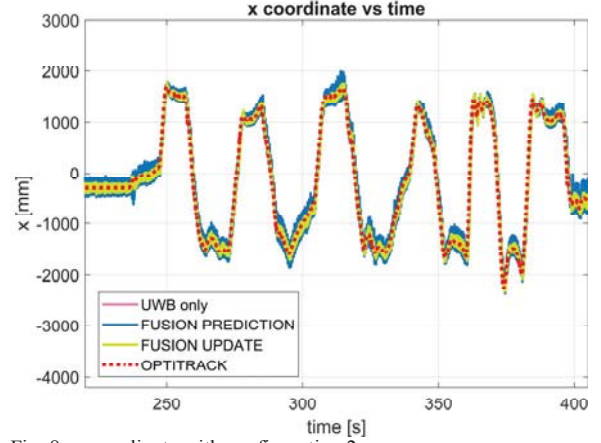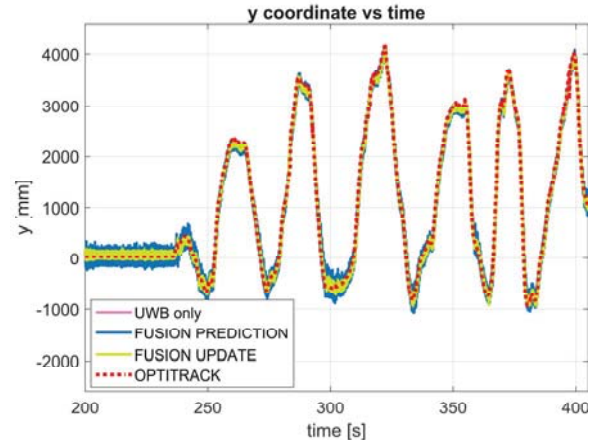
this part of the tuning process is straightforward. The hard part of the tuning process is to find out the values for the Q matrix. In our case, this task consists in finding the optimal values for the power spectral densities S_{w_x}. Even though there exist automatic procedures for setting the optimal values, in most cases it is an iterative manual process. The results presented in Fig. 10, Fig. 11, and Fig. 12 are obtained by using values of S_{w_x} that in our tuning process were found to be optimal. To evaluate the robustness of the three approaches with respect to erroneous tuning of the filter, different values of S_{w_x} were tested. While for
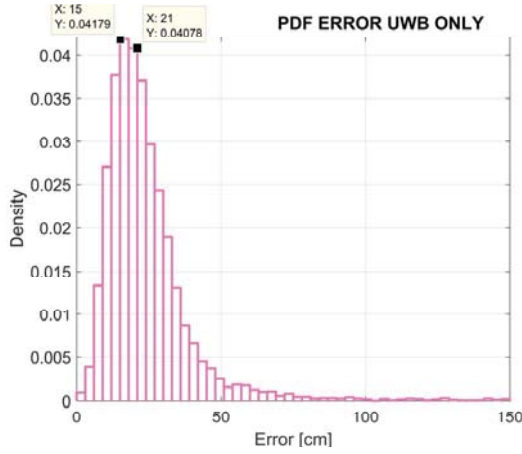
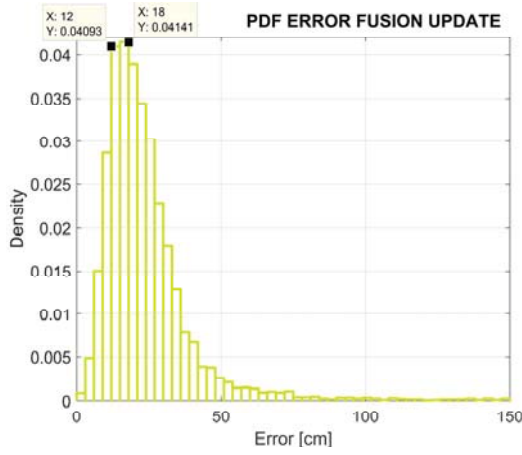Fig. 10: error probability distribution function: UWB only.

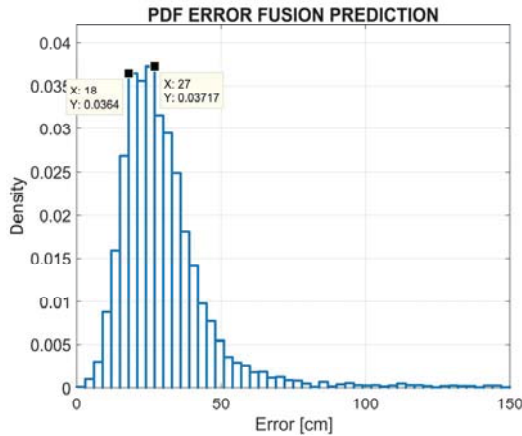Fig. 11: error probability distribution function: fusion in update step.

Fig. 12: error probability distribution function: fusion in prediction step.

Fig. 13: z coordinate with high process noise
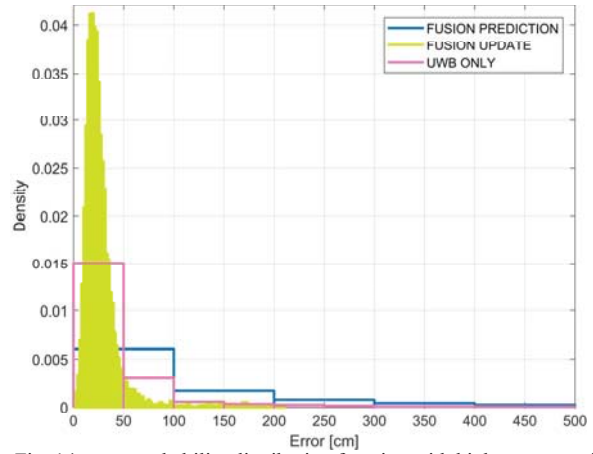
Fig. 14: error probability distribution function with high process noise.

values that were smaller than the optimal one, the PDFs of the error did not change considerably, in the case of greater values there were dramatic changes in the PDF of two of the three approaches. Fig. 13 and Fig. 14 show respectively the z coordinate and the PDF of the error for a value of the power spectral density that is hundred times bigger than the optimal value. The results show that both the solution based only on UWB data and the one that fuses IMU data in the prediction step
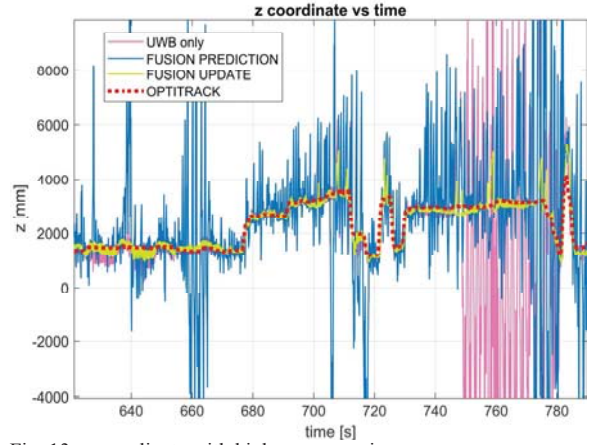
are affected by an error whose PDF is spread over hundreds of centimeters. Instead, in the case of the fusion performed in the update step, most of the PDF of the error is still concentrated below 50 cm. Moreover, the shape of the PDF is close to the case in which the optimal value was used.

VI. CONCLUSION

In this paper, we have presented a 3-D localization system that relies on the use of UWB ranging sensors. The localization is performed by using an EKF in which a "white-noise jerk model" is employed as the transition model. The advantage of this motion model is that it improves the localization performance in scenarios in which random maneuvers are performed. On the other hand, when employing the "white-noise jerk model", the EKF interprets the high process noise as strong accelerations. To counteract this phenomenon, IMU has been utilized to measure the actual accelerations. The goal of this work was to evaluate which sensor data fusion method provides better results in an architecture in which an IMU and a UWB ranging sensors are tightly coupled. The final results reveal that the fusion performed in the update step of the EKF provides higher accuracy than the fusion performed in the prediction step. The results also suggest that the integration of IMU data in the update step provides a very modest improvement of the accuracy with respect to the sole use of UWB data, while the fusion of

IMU data in the prediction step degrades the accuracy. However, the results illustrate that the use of IMU data in the update step increases the robustness of the localization system against erroneous modelling of the process noise. This last result proves that the drawback of using a CA motion model can be counteracted by integrating IMU data in the update step. By contrast, the fusion of IMU data in the prediction step not only degrades the accuracy, but it also reduces the robustness against erroneous modelling of the noise.

This work will be extended to the inclusion of different types of sensors. Furthermore, different motion models will be tested and methodology for automated tuning process of the EKF will be considered.

REFERENCES

[1] J. Xiao, Z. Liu, Y. Yang, D. Liu, and X. Han, "Comparison and analysis of indoor wireless positioning techniques," in Computer Science and Service System (CSSS), 2011 International Conference on, 2011, pp. 293–296.

[2] H. Liu, H. Darabi, P. Banerjee, and J. Liu, "Survey of wireless indoor positioning techniques and systems," IEEE Trans. Syst. Man, Cybern. Part C (Applications Rev., vol. 37, no. 6, pp. 1067–1080, 2007.

[3] J.-O. Nilsson, A. De Angelis, I. Skog, P. Carbone, and P. Händel, "Signal processing issues in indoor positioning by ultra wide band radio aided inertial navigation," in Signal Processing Conference, 2009 17th European, 2009, pp. 2161–2165.

[4] K. Pahlavan, X. Li, and J.-P. Makela, "Indoor geolocation science and technology," IEEE Commun. Mag., vol. 40, no. 2, pp. 112–118, 2002.

[5] B. Dewberry and A. Petroff, "Precision Navigation with AD-HOC Autosurvey using UltraWideBand Two-Way Ranging Network," in 12 Workshop on Positioning, Navigation and Communication (WPNC'15), 2015, pp. 1–4.

[6] M. Rhudy, J. Gross, Y. Gu, and M. Napolitano, "Fusion of GPS and redundant IMU data for attitude estimation," in AIAA Guidance, Navigation, and Control Conference, 2012, p. 5030.

[7] A. Benini, A. Mancini, A. Marinelli, and S. Longhi, "A Biased Extended Kalman Filter for indoor localization of a mobile agent using low-cost IMU and UWB wireless sensor network," IFAC Proc. Vol., vol. 45, no. 22, pp. 735–740, 2012.

[8] Q. Gan and C. J. Harris, "Comparison of two measurement fusion methods for Kalman-filter-based multisensor data fusion," IEEE Trans. Aerosp. Electron. Syst., vol. 37, no. 1, pp. 273–279, 2001.

[9] H. Choset, K. M. Lynch, S. Hutchinson, W. Kantor, George A. Burgard, L. E. Kavraki, and S. Thrun, "Kalman Filtering," in Principles of Robot Motion: Theory, Algorithms, and Implementations, MIT press, 2005, pp. 282–295.

[10] X. R. Li and V. P. Jilkov, "Survey of maneuvering target tracking. Part I. Dynamic models," IEEE Trans. Aerosp. Electron. Syst., vol. 39, no. 4, pp. 1333–1364, 2003.

[11] C. Ascher, L. Zwirello, T. Zwick, and G. Trommer, "Integrity monitoring for UWB/INS tightly coupled pedestrian indoor scenarios," in Indoor Positioning and Indoor Navigation (IPIN), 2011 International Conference on, 2011, pp. 1–6.

[12] NaturalPoint, "General FAQs," 2017. [Online]. Available: http://optitrack.com/support/faq/general.html. [Accessed: 14-Apr-2017].